Inorganic Chemistry
Article

Inorg. Chem. **2010**, *49*, 3035–3043 **3035**
DOI: 10.1021/ic902590u

Halogen Photoreductive Elimination from Metal−Metal Bonded Iridium(II)−Gold(II) Heterobimetallic Complexes

Thomas S. Teets, Daniel A. Lutterman, and Daniel G. Nocera*

Department of Chemistry, 6-335, Massachusetts Institute of Technology, 77 Massachusetts Avenue, Cambridge, Massachusetts 02139-4307

Received December 29, 2009

Halogen oxidation of $[Ir^{I}Au^{I}(dcpm)_2(CO)X](PF_6)$ (dcpm = bis(dicyclohexylphosphino)methane, X = Cl, Br) and $[Ir^{I}Au^{I}(dppm)_2(CN^{t}Bu)_2](PF_6)_2$ (dppm = bis(diphenylphosphino)methane) furnishes the heretofore unknown class of d^7—d^9 compounds comprising an $Ir^{II}Au^{II}$ heterobimetallic core. A direct metal−metal bond is evident from a 0.2 Å contraction in the intermetallic distance, as determined by X-ray crystallography. The photophysical consequence of iridium−gold bond formation, as elucidated by experimental and computational investigations, is an electronic structure dominated by a $\sigma \rightarrow \sigma^*$ transition that possesses significant ligand-to-metal charge transfer (LMCT) character. Accordingly, these compounds are non-emissive but photoreactive. Excitation of $Ir^{II}Au^{II}$ complexes in the presence of a halogen trap prompts a net photoreductive elimination of halogen and the production of the two-electron reduced $Ir^{I}Au^{I}$ species with about 10% quantum efficiency. The $Ir^{II}Au^{II}$ complexes add to a growing library of d^7—d^9 heterobimetallic species from which halogen elimination may be driven by a photon.

Introduction

Metal photocatalyzed hydrogen production from HX (X = Cl, Br) hinges upon halogen elimination via M—X bond activation.[1] This lesson is learned from the hydrogen photocycle established by bimetallic Rh complexes bridged by three bis(difluorophosphino)methylamine (dfpma) ligands.[2] A hydrido-halide $Rh_2^{II,II}(H)_2(X)_2$ species is generated from the addition of two HX molecules to a parent $Rh_2^{0,0}$ complex.[3] Whereas H_2 photoelimination is facile to furnish a two-electron $Rh_2^{0,II}(X)_2$ mixed valence complex, photoelimination of halogen from this d^7—d^9 complex is sluggish.[3,4] The overall efficiency for H_2 photogeneration has little to do with hydrogen production but rather is limited by the efficiency of halogen photoelimination to regenerate the initial photoreactant. Accordingly, recent efforts in our group have sought to develop a multielectron halogen-elimination photochemistry predicated on dissociative dσ* excited states that are heavily admixed with contributions from coordinated halide ligands. We have found that the d^7—d^9 electron count of late transition metals is particularly predisposed to halogen photoelimination. The d^7—d^9 complex $[Pt^{III}Au^{II}(dppm)_2PhCl_3]PF_6$ undergoes photochemical reduction to its $Pt^{II}Au^{I}$ precursor with a quantum yield of 5.7% when the halogen is trapped,[5] nearly a 10-fold increase over the efficiency of halogen elimination from the d^7—d^9 Rh^{II}—Rh^{0} bimetallic core. Even more efficient halogen photoelimination is achieved from more highly oxidized Pt_2 cores. $Pt_2^{III,III}(tfepma)_2Cl_6$ undergoes efficient two-electron photoreduction (Φ = 38%) at high trap concentrations, and is able to eliminate Cl_2 when irradiated in the solid state, providing what is the first example of authentic, trap-free X_2 reductive photoelimination from a transition-metal center.[6] Ligand-to-metal charge transfer (LMCT) excitation of phosphine-ligated gold(III) halide complexes that lack a metal−metal bond can also promote efficient halogen elimination from solution in the presence of trap (Φ = 26%) and from the solid state in the absence of trap.[7]

Our interest in heterobimetallic complexes stems from a desire to strike a balance in designing molecular photocatalysts that can manage the formal reduction of protons to hydrogen but at the same time are oxidizing enough to efficiently eliminate halogen to complete HX-splitting cycles. Armed with the knowledge (i) that metal−metal bonded diiridium complexes display a rich reaction chemistry with hydrohalic acids and reversibly add hydrogen[8] and (ii) that

*To whom correspondence should be addressed. E-mail: nocera@mit.edu.

(1) Esswein, A. J.; Nocera, D. G. *Chem. Rev.* **2007**, *107*, 4022–4047.
(2) Heyduk, A. F.; Nocera, D. G. *Science* **2001**, *293*, 1639–1641.
(3) Esswein, A. J.; Veige, A. S.; Nocera, D. G. *J. Am. Chem. Soc.* **2005**, *127*, 16641–16651.
(4) Odom, A. L.; Heyduk, A. F.; Nocera, D. G. *Inorg. Chim. Acta* **2000**, *297*, 330–337.
(5) Cook, T. R.; Esswein, A. J.; Nocera, D. G. *J. Am. Chem. Soc.* **2007**, *129*, 10094–10095.
(6) Cook, T. R.; Surendranath, Y.; Nocera, D. G. *J. Am. Chem. Soc.* **2009**, *131*, 28–29.
(7) Teets, T. S.; Nocera, D. G. *J. Am. Chem. Soc.* **2009**, *131*, 7411–7420.
(8) Heyduk, A. F.; Nocera, D. G. *J. Am. Chem. Soc.* **2000**, *122*, 9415–9426.

Published on Web 02/18/2010

complexes containing more oxidizing transition metals efficiently eliminate halogen (vide supra), we turned our attention to iridium−gold heterobimetallic complexes as promising candidates as next-generation HX-splitting catalysts.

Iridium(I)−gold(I) heterobimetallic complexes were first reported by Shaw and co-workers, who detailed the synthesis of $[Ir^IAu^I(dppm)_2COCl]Cl$,[9] and later described synthetic methods for substituting methyl isocyanide (MeNC) onto the iridium center.[10] Since these initial reports, photophysical[11−14] and computational studies[15] of Ir^IAu^I complexes have emerged, though the reactivity of these complexes remains underexplored. Reactions with select Lewis acids such as $HgCl_2$ and BF_3 have been characterized for $[Ir^IAu^I(dppm)_2COCl](PF_6)$[16] and a trimetallic $Ir^IAu^IIr^I$ complex has been oxidized.[17] But oxidative-addition to bimetallic iridium−gold species has not been detailed, and photochemical transformations involving iridium−gold heterobimetallics are likewise unknown.

In this work, we describe the synthesis of d^8—d^{10} Ir^IAu^I complexes spanned by two bridging diphosphines. Oxidation with halogen furnishes the d^7—d^9 $Ir^{II}Au^{II}$ bimetallic complex; this electron count has heretofore not been observed for Ir bonded to Au. The complexes possess a formal metal−metal σ-bond, which is validated by structural metrics from X-ray crystallography. Experimental and computational studies establish an electronic structure that is dominated by $d\sigma \rightarrow d\sigma^*$ character with significant halide admixture. Consistent with this bonding formulation, irradiation of the $Ir^{II}Au^{II}$ complexes activates M—X bonds, and halogen photoreductive elimination is achieved.

Experimental Section

General Considerations. All reactions involving air-sensitive materials were executed in a nitrogen-filled glovebox using solvents previously dried by passage through an alumina column under argon. The starting materials bis(dicyclohexylphosphino)methane (dcpm) and $[Ir^I(COD)Cl]_2$ (COD = 1,5-cyclooctadiene) were obtained from Strem, and bromine and *tert*-butylisocyanide (CN^tBu) were obtained from Sigma-Aldrich. Chlorine was delivered as the iodobenzene adduct $PhICl_2$.[18] $[Ir^I(dcpm)_2CO]Cl$ and $[Ir^I(dcpm)_2CO]Br$ were prepared in an analogous fashion to that described for $[Ir^I(dppm)_2CO]Cl$.[19,20] Gold(I) starting materials $Au^I(tht)Cl$ (tht = tetrahydrothiophene) and $Au^I(tht)Br$ were synthesized as previously described.[21] For additions of Br_2 to reactions, a stock solution was prepared using a weighed amount of bromine, and then an appropriate aliquot was added using an autopipet.

Physical Methods. All NMR spectra were recorded at the MIT Department of Chemistry Instrumentation Facility on a Varian Mercury 300 NMR Spectrometer or a Varian Inova-500 NMR Spectrometer. $^{31}P\{^1H\}$ NMR spectra were referenced to an external standard of 85% D_3PO_4, and ^1H spectra were referenced to tetramethylsilane (TMS) using the residual proteo solvent resonances. UV−vis spectra were recorded at 293 K in CH_2Cl_2 solutions in quartz cuvettes on a Varian Cary 5000 UV−vis−NIR spectrophotometer. Extinction coefficients were determined over a concentration range of ~2−50 μM, for which all compounds obeyed Beer's Law. Steady state emission spectra were recorded on an automated Photon Technology International (PTI) QM 4 fluorimeter equipped with a 150-W Xe arc lamp and a Hamamatsu R928 photomultiplier tube. Excitation light was excluded with appropriate glass filters. Samples were housed in custom quartz EPR tubes with a ground-glass joint and Teflon plug. Solution samples were prepared in 1:1 CH_2Cl_2/toluene and freeze pump thaw degassed (4 cycles, 1×10^{-5} torr). Solid samples were prepared by evaporation of a CH_2Cl_2 solution under vacuum; the resulting solid film was evacuated to $< 1 \times 10^{-5}$ torr. Spectra were recorded at 77 K by immersion of the sealed EPR tubes into a liquid nitrogen filled quartz dewar flask. Time resolved phosphorescence lifetimes were recorded on a nanosecond laser system described previously.[22] IR spectra of powdered samples were recorded on a PerkinElmer Spectrum 400 FT-IR/FT-FIR Spectrometer outfitted with a Pike Technologies GladiATR attenuated total reflectance accessory with a monolithic diamond crystal stage and pressure clamp.

Photochemistry. Photochemical reactions were performed using a 1000 W high-pressure Hg/Xe arc lamp (Oriel). The beam was passed through a water-jacketed filter holder containing appropriate long pass filters, an iris and collimating lens. Samples for all photolysis experiments were prepared in a nitrogen-filled glovebox in quartz cuvettes equipped with a magnetic stir bar and a threaded screw-cap and kept rigorously excluded from light until the start of irradiation. Monochromatic light was generated by combining the output from a long-pass filter with a Hg line filter of the appropriate wavelength. For quantum yield measurements, potassium ferrioxalate was synthesized via a published procedure and used as a chemical actinometer.[23] The photon flux was determined from the average of the actinometric measurements collected before and after irradiation of a set of six samples. UV−vis spectra for steady-state photolysis experiments and quantum yield measurements were recorded on a Spectral Instruments 400 diode array spectrophotometer and were blanked to the appropriate solvent.

Computational Methods. All calculations were performed using the Gaussian 03 program suite.[24] Where possible, atomic coordinates for geometry optimizations originated from X-ray diffraction data. Cyclohexyl, phenyl, and *tert*-butyl groups were replaced with methyl groups, and counterions were omitted. Density functional theory (DFT) calculations were carried out using the three hybrid functionals of Becke[25] in conjunction with the correlation functional of Lee, Yang, and Parr (B3LYP).[26,27] The 6-31G(p,d) basis set was applied to all non-metal atoms,[28,29] and the Stuttgart effective core potential and associated basis set was used for Ir and Au.[30] All calculations were spin-restricted on

(9) Hutton, A. T.; Pringle, P. G.; Shaw, B. L. *Organometallics* **1983**, *2*, 1889–1891.
(10) Langrick, C. R.; Shaw, B. L. *J. Chem. Soc., Dalton Trans.* **1985**, 511–516.
(11) Balch, A. L.; Catalano, V. J.; Olmstead, M. M. *Inorg. Chem.* **1990**, *29*, 585–586.
(12) Balch, A. L.; Catalano, V. J. *Inorg. Chem.* **1991**, *30*, 1302–1308.
(13) Striplin, D. R.; Brozik, J. A.; Crosby, G. A. *Chem. Phys. Lett.* **1994**, *231*, 159–163.
(14) Striplin, D. R.; Crosby, J. A. *J. Phys. Chem.* **1995**, *99*, 7977–7984.
(15) Liu, T.; Zhou, X.; Zhang, H.-X.; Xia, B.-H. *Dalton. Trans.* **2008**, 1065–1072.
(16) Balch, A. L.; Catalano, V. J. *Inorg. Chem.* **1992**, *31*, 2730–2734.
(17) Balch, A. L.; Nagle, J. K.; Oram, D. E.; Reedy, P. E., Jr. *J. Am. Chem. Soc.* **1988**, *110*, 454–462.
(18) Zielinska, A.; Skulski, L. *Tetrahedron Lett.* **2004**, *45*, 1087–1089.
(19) Miller, J. S.; Caulton, K. G. *J. Am. Chem. Soc.* **1975**, *97*, 1067–1073.
(20) Vaska, L.; Catone, D. L. *J. Am. Chem. Soc.* **1966**, *88*, 5324–5325.
(21) Usón, R.; Laguna, A.; Laguna, M. *Inorg. Synth.* **1989**, *26*, 85–91.
(22) Loh, Z.-H.; Miller, S. E.; Chang, C. J.; Carpenter, S. D.; Nocera, D. G. *J. Phys. Chem. A* **2002**, *106*, 11700–11708.
(23) Montalti, M.; Credi, A.; Prodi, L.; Gandolfi, M. T. *Handbook of Photochemistry*, 3rd ed.; Taylor and Francis: Boca Raton, FL, 2006.
(24) *Gaussian 03*, Revision D.01; Gaussian, Inc.: Wallingford, CT, 2004; Full citation in the Supporting Information.
(25) Becke, A. D. *J. Chem. Phys.* **1993**, *98*, 5648–5652.
(26) Lee, C.; Yang, W.; Parr, R. G. *Phys. Rev. B* **1988**, *37*, 785–789.
(27) Miehlich, B.; Savin, A.; Stoll, H.; Preuss, H. *Chem. Phys. Lett.* **1989**, *157*, 200–206.
(28) Hariharan, P. C.; Pople, J. A. *Theor. Chim. Acta* **1973**, *28*, 213–222.
(29) Francl, M. M.; Pietro, W. J.; Hehre, W. J.; Binkley, J. S.; Gordon, M. S.; DeFrees, D. J.; Pople, J. A. *J. Chem. Phys.* **1982**, *77*, 3654–3655.
(30) Dolg, M.; Wedig, U.; Stoll, H.; Preuss, H. *J. Chem. Phys.* **1987**, *86*, 866–872.

gas-phase molecules, with no imposed symmetry. Time dependent calculations were initiated from the optimized geometry using the B3LYP exchange and correlation functionals. Molecular orbitals were imaged in the program GaussView 3.0 with an isodensity of 0.04 applied. Optimized Cartesian coordinates for the model compounds considered here are deposited in the Supporting Information.

Preparation of $[Ir^{I}Au^{I}(dcpm)_2COCl](PF_6)$ (1). To a solution of $[Ir^{I}(dcpm)_2CO]Cl$ (1.00 g, 0.932 mmol) in 6 mL of CH_2Cl_2 was added a solution of Au(tht)Cl (299 mg, 0.932 mmol) in 8 mL of CH_2Cl_2. The orange solution was stirred at room temperature for 1 h, at which time a solution of NH_4PF_6 (228 mg, 1.40 mmol) in 15 mL of methanol was added. The solution was concentrated to <10 mL via rotary evaporation, during which time and orange solid precipitated. The solid was collected by filtration, washed with 5 mL of methanol and dried in vacuo. Yield: 1.04 g (78.8%). ^{1}H NMR (500 MHz, CD_2Cl_2) δ/ppm: 2.50−2.69 (br, m, 6H), 2.33 (br, d, 2H), 2.17−2.29 (br, m, 4H), 1.14−2.09 (br, m, 80H). $^{31}P\{^1H\}$ NMR (121.5 MHz, CD_2Cl_2) δ/ppm: 51.0 (m, 2P), 25.3 (m, 2P), −144.1 (sept., $^1J_{P-F}$ = 711 Hz, 1P). UV−vis (CH_2Cl_2): λ/nm $\{\varepsilon/(M^{-1}\ cm^{-1})\}$ 300 (sh) {4300}, 316 {5700}, 355 {2500}, 431 {17000}, 517 {300}. IR (solid): $\tilde{\nu}_{CO}$ = 1944 cm^{-1}. Anal. Calcd. for $C_{51}H_{92}AuClF_6IrOP_5$: C, 43.30; H, 6.55. Found: C, 43.37; H, 6.51.

Preparation of $[Ir^{I}Au^{I}(dcpm)_2COBr](PF_6)$ (2). A solution of Au(tht)Br (327 mg, 0.895 mmol) in 8 mL of CH_2Cl_2 was added to a solution of $[Ir^{I}(dcpm)_2CO]Br$ (1.00 g, 0.0895 mmol) in 6 mL of CH_2Cl_2. The resulting dark orange solution was stirred for 90 min at room temperature and then filtered through a plug of glass wool. A solution of NH_4PF_6 (220 mg, 1.35 mmol) in 15 mL of methanol was added, and the resulting bright orange solution was stirred for 1 h. After concentrating to <10 mL by rotary evaporation, an orange solid formed, which was collected by filtration, washed with 10 mL of methanol, and dried in vacuo. Yield: 1.14 g (87.0%). ^{1}H NMR (500 MHz, CD_2Cl_2) δ/ppm: 2.50−2.82 (br, m, 6H), 2.15−2.40 (br, m, 6H), 1.00−2.10 (br, m, 80H). $^{31}P\{^1H\}$ NMR (121.5 MHz, CD_2Cl_2) δ/ppm: 50.4 (m, 2P), 23.2 (m, 2P), −144.2 (sept., $^1J_{P-F}$ = 711 Hz, 1P). UV−vis (CH_2Cl_2): λ/nm $\{\varepsilon/(M^{-1}\ cm^{-1})\}$ 307 (sh) {5800}, 319 {6400}, 360 {2600}, 437 {18000}, 526 {320}. IR (solid): $\tilde{\nu}_{CO}$ = 1945 cm^{-1}. Anal. Calcd. for $C_{51}H_{92}AuBrF_6IrOP_5$: C, 41.98; H, 6.35. Found: C, 41.90; H, 6.36.

Preparation of $[Ir^{I}Au^{I}(dppm)_2(CN^{t}Bu)_2](PF_6)_2$ (3). To a solution of $[Ir(COD)Cl]_2$ (149 mg, 0.222 mmol) in 5 mL of CH_2Cl_2 was added a solution of dppm (341 mg, 0.887 mmol) in 2 mL of CH_2Cl_2, giving a yellow solution. A solution of $CN^{t}Bu$ (73.7 mg, 0.887 mmol) was added immediately, initially causing a change to a lighter yellow color, which darkened to yellow-orange as the solution was stirred for 20 min. At this time, a solution of Au(tht)Cl (142 mg, 0.443 mmol) in 2 mL of CH_2Cl_2 was added, giving a deep red solution which was stirred for 45 min. Addition of a solution of NH_4PF_6 (180 mg, 1.10 mmol) in 20 mL of MeOH prompted an instantaneous color change to dark green. The solution was concentrated to 5 mL, and the resulting green solid was filtered and washed with 5 mL of methanol. The crude solid was dissolved in 2 mL of CH_2Cl_2 and recrystallized by layering with 1 mL of methanol followed by 17 mL of diethyl ether. After several hours, green microcrystals formed, which were separated from the supernatant by decantation and dried in vacuo. Yield: 382 mg (53.4%). ^{1}H NMR (500 MHz, CD_2Cl_2) δ/ppm: 7.84−7.90 (m, 8H), 7.68−7.74 (m, 8H), 7.52−7.63 (m, 12H), 7.44−7.50 (m, 4H), 7.38−7.43 (m, 8H), 4.10 (br, pseudoquintet, 4H), 0.63 (s, 18H). $^{31}P\{^1H\}$ NMR (202.5 MHz, CD_2Cl_2) δ/ppm: 30.0 (m, 2P), 10.4 (m, 2P), −143.9 (sept., $^1J_{P-F}$ = 712 Hz, 2P). UV−vis (CH_2Cl_2): λ/nm $\{\varepsilon/(M^{-1}\ cm^{-1})\}$ 345 {11000}, 402 {4400}, 490 {26000}, 606 {520}. IR (solid): $\tilde{\nu}_{CN}$= 2138 cm^{-1}. Anal. Calcd. for $C_{60}H_{62}AuF_{12}IrN_2P_6$: C, 44.65; H, 3.87; N, 1.74. Found: C, 44.39; H, 3.82; N, 1.59.

Preparation of $[Ir^{II}Au^{II}(dcpm)_2COCl_3](PF_6)$ (4). A solution of **1** (100 mg, 0.0707 mmol) in 1.5 mL of CH_2Cl_2 and a solution of $PhICl_2$ (23.3 mg, 0.0848 mmol, 1.20 equiv) in 0.7 mL of CH_2Cl_2 were both chilled with liquid N_2 in the glovebox cold well. Once frozen, the two samples were removed, and upon melting the $PhICl_2$ solution was added dropwise to the solution of **1**. The color immediately faded to a lighter orange, and the solution was stirred at room temperature for 3 h. Dropwise addition of 15 mL of pentane to the stirred solution yielded a yellow-orange solid, which was separated from the supernatant by decantation and dried in vacuo. Yield: 104 mg (99.0%). ^{1}H NMR (500 MHz, CD_2Cl_2) δ/ppm: 3.62−3.73 (m, 2H), 3.08−3.22 (br, m, 4H), 2.81−2.90 (br, m, 2H), 2.68−2.77 (br, m, 2H), 2.54−2.64 (br, m, 2H), 2.44−2.51 (br, m, 2H), 2.08−2.32 (br, m, 6H), 1.20−2.05 (br, m, 72H). $^{31}P\{^1H\}$ NMR (121.5 MHz, CD_2Cl_2) δ/ppm: 31.6 (pseudotriplet, 2P), −11.0 (pseudotriplet, 2P), −144.1 (sept., $^1J_{P-F}$ = 714 Hz, 1P). UV−vis (CH_2Cl_2): λ/nm $\{\varepsilon/(M^{-1}\ cm^{-1})\}$ 266 {22000}, 331 {23000}, 396 {5800} 455 (sh) {1200}. IR (solid): $\tilde{\nu}_{CO}$ = 2009 cm^{-1}. Anal. Calcd. for $C_{51}H_{92}AuCl_3F_6IrOP_5$: C, 41.23; H, 6.24. Found: C, 40.96; H, 6.15.

Preparation of $[Ir^{II}Au^{II}(dcpm)_2COBr_3](PF_6)$ (5). A sample of **2** (100 mg, 0.0685 mmol) was dissolved in 4 mL of acetonitrile. A solution of Br_2 (11.5 mg, 0.0720 mmol, 1.05 equiv) in 0.3 mL of acetonitrile was added dropwise. The resulting suspension was stirred at room temperature for 30 min. All volatiles were removed by rotary evaporation to afford an orange solid, which was suspended in 15 mL of diethyl ether and collected by filtration. The product was washed with 10 mL of diethyl ether and dried in vacuo. Yield: 97 mg (87%). ^{1}H NMR (500 MHz, CD_2Cl_2) δ/ppm: 3.84−3.94 (m, 2H), 3.35−3.49 (br, m, 4H), 2.88−2.96 (br, m, 2H), 2.73−2.81 (br, m, 2H), 2.33 (br, d, 2H) 2.24 (br, d, 2H), 2.08 (br, d, 2H), 1.21−2.05 (br, m, 76H). $^{31}P\{^1H\}$ NMR (121.5 MHz, CD_2Cl_2) δ/ppm: 25.7 (pseudotriplet, 2P), −18.6 (pseudotriplet, 2P), −144.2 (sept., $^1J_{P-F}$ = 711 Hz, 1P). UV−vis (CH_2Cl_2): λ/nm $\{\varepsilon/(M^{-1}\ cm^{-1})\}$ 283 (sh) {16000}, 305 {23000}, 369 {15000}, 416 (sh) {9400}, 496 (sh) {1500}. IR (solid): $\tilde{\nu}_{CO}$ = 2007 cm^{-1}. Anal. Calcd. for $C_{51}H_{92}AuBr_3F_6IrOP_5$: C, 37.83; H, 5.73. Found: C, 37.59; H, 5.64.

Preparation of $[Ir^{II}Au^{II}(dppm)_2(CN^{t}Bu)_2Cl_2](PF_6)_2$ (6). A solution **3** (100 mg, 0.0620 mmol) in 1.5 mL of CH_2Cl_2 and a solution of $PhICl_2$ (18 mg, 0.065 mmol, 1.2 equiv) in 1 mL of CH_2Cl_2 were prepared and frozen in the glovebox cold well. After removing from the cold well and allowing the solution to melt, the $PhICl_2$ solution was added dropwise, prompting an immediate color change from dark green to bright yellow. The reaction solution was stirred in the dark for 1 h. The yellow solution was filtered through a plug of glass wool into 18 mL of pentane, which resulted in the formation of a pale yellow powder. The supernatant was decanted, and the remaining solid was washed with pentane and dried in vacuo. Yield: 94 mg (90%). ^{1}H NMR (500 MHz, CD_2Cl_2) δ/ppm: 7.61−7.70 (br, m, 16H), 7.46−7.56 (br, m, 24H), 5.24 (br, pseudoquintet, 4H), 1.01 (s, 18H). $^{31}P\{^1H\}$ NMR (121.5 MHz, CD_2Cl_2) δ/ppm: 7.7 (pseudotriplet, 2P), −17.6 (pseudotriplet, 2P), −143.9 (sept., $^1J_{P-F}$ = 711 Hz, 2P). UV−vis (CH_2Cl_2): λ/nm $\{\varepsilon/(M^{-1}\ cm^{-1})\}$ 257 {34000}, 320 {33000}, 388 (sh) {2600}. IR (solid): $\tilde{\nu}_{CN}$ = 2192 cm^{-1}. Anal. Calcd. for $C_{60}H_{62}AuCl_2F_{12}IrN_2P_6$: C, 42.77; H, 3.71; N, 1.66. Found: C, 42.43; H, 3.87; N, 1.60.

Preparation of $[Ir^{II}Au^{II}(dppm)_2(CN^{t}Bu)_2Br_2](PF_6)_2$ (7). A 10 mL Schlenk tube was charged with a solution of **3** (100 mg, 0.0620 mmol) in 2 mL of CH_2Cl_2 and chilled to −78 °C under an argon atmosphere. A solution of Br_2 (10.4 mg, 0.0650 mmol, 1.05 equiv) in 228 μL of CH_2Cl_2 was added dropwise, causing an immediate color change to pale orange. The solution was allowed to warm to room temperature and stirred for 15 min. Addition of 17 mL of pentane afforded a yellow-orange solid, which was separated by decanting the supernatant and dried in vacuo. Yield: 106 mg (96.4%). ^{1}H NMR (500 MHz, CD_2Cl_2) δ/ppm: 7.61−7.69 (br, m, 16H), 7.35−7.60 (br, m, 24H), 5.33−5.37 (br, m, 4H), 1.06 (s, 18H). $^{31}P\{^1H\}$ NMR (202.5 MHz, CD_2Cl_2) δ/ppm: 3.1 (pseudotriplet, 2P), −22.2 (pseudotriplet, 2P), −143.9 (sept., $^1J_{P-F}$ = 712 Hz, 2P). UV−vis (CH_2Cl_2): λ/nm $\{\varepsilon/(M^{-1}\ cm^{-1})\}$ 255 (sh) {34000}, 344

Table 1. Crystallographic Summary for Complexes **1**, **2**, **4**, **5**, **6**, **7**

	1	**2**·Et_2O	**4**·CH_2Cl_2	**5**·CH_2Cl_2	**6**·$2CH_2Cl_2$	**7**·$2CH_2Cl_2$
formula	$C_{51}H_{92}AuClF_6IrOP_5$	$C_{55}H_{102}AuBrF_6IrO_2P_5$	$C_{52}H_{94}AuCl_5F_6IrOP_5$	$C_{52}H_{94}AuBr_3Cl_2F_6IrOP_5$	$C_{62}H_{66}AuC_{16}F_{12}IrN_2P_6$	$C_{62}H_{66}AuBr_2Cl_4F_{12}IrN_2P_6$
fw, g/mol	1414.71	1533.29	1570.54	1703.92	1854.85	1943.77
temperature	100(2) K	100(2) K	100(2) K	100(2) K	100(2) K	100(2) K
cryst. syst.	monoclinic	monoclinic	monoclinic	monoclinic	monoclinic	monoclinic
space group	$P2_1/c$	$P2_1/n$	$P2_1/c$	$P2_1/c$	$P2_1/c$	$P2_1/c$
color	orange	orange	orange	orange	yellow	orange
a (Å)	13.5909(13)	15.0304(16)	14.5925(16)	14.6114(14)	16.551(2)	16.4460(18)
b (Å)	22.404(2)	21.199(2)	20.500(2)	20.703(2)	20.888(3)	20.891(2)
c (Å)	18.9079(17)	20.366(2)	20.651(2)	20.627(2)	21.963(3)	22.145(2)
α (deg)	90	90	90	90	90	90
β (deg)	94.232(2)	102.708(2)	95.279(2)	95.402(2)	106.100(2)	105.181(2)°.
γ (deg)	90	90	90	90	90	90
V (Å^3)	5741.6(9)	6330.3(11)	6151.7(11)	6212.0(10)	7295.4(17)	7343.1(14)
Z	4	4	4	4	4	4
$R1$[a] (all data)	0.0416	0.0356	0.0474	0.0534	0.0582	0.0690
$wR2$[b] (all data)	0.0702	0.0669	0.0826	0.0839	0.1000	0.1070
$R1$ [$(I > 2\sigma)$]	0.0305	0.0278	0.0348	0.0351	0.0399	0.0417
$wR2$ [$(I > 2\sigma)$]	0.0657	0.0636	0.0765	0.0759	0.0894	0.0931
GOF[c]	1.070	1.049	1.051	1.012	1.038	1.023

[a] $R1 = \sum||F_o| - |F_c||/\sum|F_o|$. [b] $wR2 = [\sum w(F_o^2 - F_c^2)^2/\sum w(F_o^2)^2]^{1/2}$. [c] GOF $= [\sum w(F_o^2 - F_c^2)^2/(n-p)]^{1/2}$ where n is the number of data and p is the number of parameters refined.

{38000}. IR (solid): $\tilde{\nu}_{CN}$ = 2189 cm^{-1}. Anal. Calcd. for $C_{60}H_{62}AuBr_2F_{12}IrN_2P_6$: C, 40.62; H, 3.52; N, 1.58. Found: C, 40.63; H, 3.62; N, 1.45.

X-ray Crystallographic Details. Single crystals of **1** and **2** were obtained by vapor diffusion of diethyl ether into an acetonitrile solution, crystals of **4** were grown by layering a CH_2Cl_2 solution with methanol/diethyl ether, and crystals of **5**, **6**, and **7** were obtained from CH_2Cl_2 solutions layered with diethyl ether. The crystals were mounted on a Bruker three circle goniometer platform equipped with an APEX detector. A graphic monochromator was employed for wavelength selection of the Mo Kα radiation (λ = 0.71073 Å). The data were processed and refined using the program SAINT supplied by Siemens Industrial Automation. Structures were solved by direct methods in SHELXS and refined by standard difference Fourier techniques in the SHELXTL program suite (6.10 v., Sheldrick G. M., and Siemens Industrial Automation, 2000). Hydrogen atoms were placed in calculated positions using the standard riding model and refined isotropically; all other atoms were refined anisotropically. A positional disorder of the CO ligand and the halide *trans* to it was present in the structures of **1**, **2**, **4**, and **5**. The thermal displacement parameters of the CO ligand in the minor disordered component were constrained to be identical to those of the CO ligand in the major component. The structures of **5**, **6**, and **7** all contained one dichloromethane solvate molecule that was modeled as a two-part disorder. In **6**, one of the two *tert*-butyl groups was found to be disordered over two sites. The checkCIF reports for isostructural **6** and **7** each indicated analogous level A alerts; one can be attributed to thermal motion in *tert*-butyl groups which were not able to be satisfactorily modeled as two-part disorders, and the other is a close intermolecular contact caused by substantial disorder in the dichloromethane solvate molecules. The (1,2) and (1,3) distances of all disordered parts were restrained to be similar using the SADI command; the rigid-bond restraints SIMU and DELU were also used on disordered parts. Unit cell parameters, morphology, and solution statistics for the structures of **1**, **2**, **4**, 5, **6**, and **7** are summarized in Table 1 below. All thermal ellipsoid plots are drawn at 50% probability level, with hydrogen atoms, counterions, and solvent molecules omitted.

Results

Synthesis and Characterization. Ir^IAu^I compounds were synthesized by following the route depicted in Scheme 1. The complexes $[Ir^IAu^I(dcpm)_2(CO)X](PF_6)$ [X = Cl (**1**), Br (**2**)] are prepared by a method similar to that used for the synthesis of the dppm-bridged complex.[9] Reaction of $[Ir^I(dcpm)_2CO]X$ with Au(tht)X in CH_2Cl_2, followed by anion exchange with methanolic NH_4PF_6, affords **1** and **2** as bright orange solids. The ^{1}H NMR spectra of **1** and **2** are not particularly informative, consisting mainly of broad, overlapping cyclohexyl resonances. The identity and purity of these compounds are most readily established by ^{31}P NMR. In the $^{31}P\{^1H\}$ spectrum of both **1** and **2**, 14 of the 20 possible lines resulting from the AA′XX′ spin system can be resolved, and the position of the two frequencies is responsive to halide substitution. The two peaks in the spectrum of **1**, centered at 51.0 and 25.3 ppm, shift to 50.4 and 23.2 ppm in **2**. The larger shift of the upfield resonance suggests that it originates from the phosphorus atoms bound to iridium, which is the site of the halide substitution. Complexes **1** and **2** also possess distinctive C≡O IR stretching frequencies at 1944 cm^{-1} (**1**) and 1945 cm^{-1} (**2**), which are invariant to halide substitution.

Scheme 1

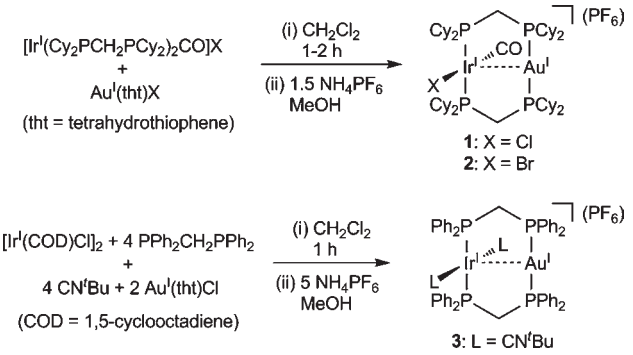

An Ir^IAu^I complex, with isocyanide ligands on the iridium, was also prepared. Though the methyl isocyanide complex $[Ir^IAu^I(dppm)_2(CNMe_2)](PF_6)_2$ was reported by Shaw and co-workers,[10] we opted to prepare the *tert*-butyl isocyanide (CN^tBu) complex owing to the

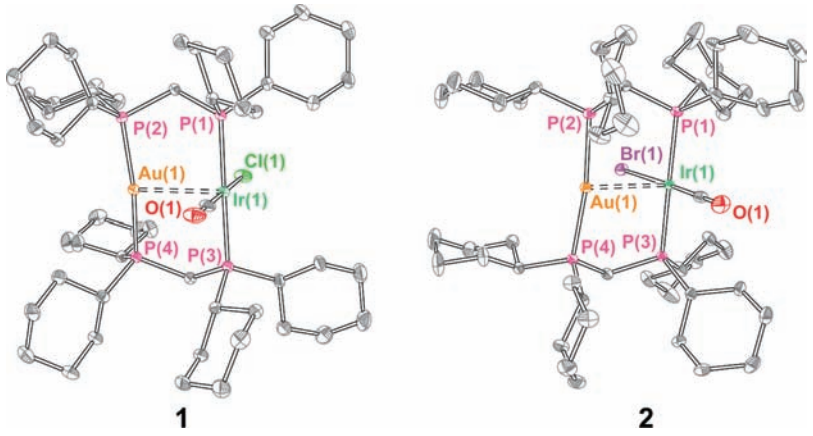

Figure 1. Thermal ellipsoid plots for **1** and **2**. Ellipsoids are shown at 50% probability level with counterions, solvent molecules, and hydrogen atoms omitted for clarity. Data was collected at 100 ± 2 K. The metal−metal distance is *d*(Ir···Au) = 2.9411(3) Å for **1** and *d*(Ir···Au) = 2.9174(2) Å for **2**.

commercial availability of this isocyanide. The desired $[Ir^{I}Au^{I}(dppm)_2(CN^{t}Bu)_2]^{2+}$ product, which can be isolated as its green PF_6^- salt (**3**), is obtained in moderate yields in a stepwise fashion starting with $[Ir(COD)Cl]_2$, which reacts sequentially with stoichiometric amounts of dppm, $CN^{t}Bu$, and Au(tht)Cl. The $^{31}P\{^{1}H\}$ NMR spectrum of **3** shows a complex splitting pattern, with two multiplets centered at 30.0 and 10.4 ppm. As with **1** and **2**, 14 of the 20 lines can be discerned. The splitting pattern is distinct from that of **1** and **2**, however, because the two outermost lines of each 7-line multiplet are the most intense. Complex **3** shows a characteristic C≡N stretch in the IR spectrum at 2138 cm^{-1}.

Compounds **1** and **2** were structurally characterized by X-ray crystallography. Table 1 summarizes crystallographic data for **1**, **2**, and **4**−**7**. The thermal ellipsoid plots of the structures of **1** and **2**, shown in Figure 1, exhibit the expected square planar coordination environment for d^8 Ir^{I} and linear geometry for d^{10} Au^{I}. The Ir···Au distance changes minimally with halide substitution, contracting by < 0.03 Å when the chloride (in **1**) is replaced with a bromide (in **2**). The Ir···Au distances in **1** and **2** are slightly shorter than the distance of 2.986(1) Å reported for the dppm-bridged analogue $[Ir^{I}Au^{I}(dppm)_2COCl](PF_6)$.[11] Complex **3** eluded structural characterization, but the related complex $[Ir^{I}Au^{I}(dppm)_2(CNMe_2)](PF_6)_2$ has a reported Ir···Au distance of 2.944(1) Å.[12]

Whereas treatment of the known complex $[Ir^{I}Au^{I}(dppm)_2COCl](PF_6)$[9] with $PhICl_2$ leads to a mixture of two products that decompose in a matter of hours to an intractable white solid, treatment of complexes **1**−**3** with $PhICl_2$ or Br_2 leads to a clean two-electron oxidation that quantitatively furnishes d^7—d^9 $Ir^{II}Au^{II}$ complexes. The complexes $[Ir^{II}Au^{II}(dcpm)_2(CO)X_3](PF_6)$ (X = Cl (**4**); Br (**5**)) and $[Ir^{II}Au^{II}(dppm)_2(CN^{t}Bu)_2X_2](PF_6)_2$ (X = Cl (**6**); Br (**7**)) were prepared in good isolated yields by halogen oxidation of the appropriate $Ir^{I}Au^{I}$ starting material. Scheme 2 summarizes the syntheses of these complexes where X_2 refers to the halogen oxidant, either $PhICl_2$ or Br_2. Oxidation of the $Ir^{I}Au^{I}$ complexes results in a sizable upfield shift of the $^{31}P\{^{1}H\}$ spectrum, which for the $Ir^{II}Au^{II}$ complexes consists of two deceptively simple AA′XX′ 1:2:1 triplets where only 6 of the 20 lines of the AA′XX′ splitting pattern are resolved. The AA′XX′ triplets undergo a significant upfield shift upon substituting chloride for bromide in otherwise identical

Scheme 2

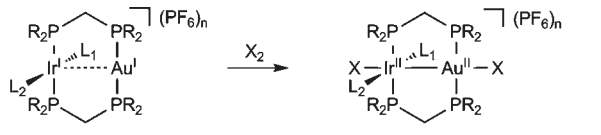

1: L_1 = CO; L_2 = Cl; R = Cy; n = 1
2: L_1 = CO; L_2 = Br; R = Cy; n = 1
3: $L_1 = L_2 = CN^{t}Bu$; R = Ph; n = 2

4: L_1 = CO; L_2 = X = Cl; R = Cy; n = 1
5: L_1 = CO; L_2 = X = Br; R = Cy; n = 1
6: $L_1 = L_2 = CN^{t}Bu$; X = Cl; R = Ph; n = 2
7: $L_1 = L_2 = CN^{t}Bu$; X = Br; R = Ph; n = 2

complexes. Resonances at 31.6 and −11.0 ppm in the ^{31}P NMR spectrum of **4** shift to 25.7 and −18.6 ppm in bromide-substituted **5**. Similarly, peaks at 7.7 and −17.6 ppm in the spectrum of **6** shift upfield to 3.1 and −22.2 ppm for bromide complex **7**. This substantial perturbation of both ^{31}P resonances is consistent with halogen ligation of both metal centers. Complexes **4**−**7** also possess distinct C≡O or C≡N stretching frequencies, which appear at 2009 (**4**), 2007 (**5**), 2192 (**6**), and 2189 cm^{-1} (**7**). These IR stretches are independent of the identity of the halogen ligands.

Structural characterization of **4**−**7** confirms the assignment of these products as metal−metal bonded $Ir^{II}Au^{II}$ complexes. Thermal ellipsoid plots for **4**−**7** are depicted in Figure 2. Clearly evident are the octahedral and square planar coordination environments of the d^7 Ir^{II} and the d^9 Au^{II} centers, respectively. Furthermore, a significant contraction in the Ir−Au bond distance is observed upon oxidation. For the $[Ir^{II}Au^{II}(dcpm)_2(CO)X_3](PF_6)$ series, the Ir−Au bond lengths of 2.6954(3) Å (**4**) and 2.7096(4) Å (**5**) are > 0.2 Å shorter than those of their precursors **1** and **2**. The metal−metal bond lengths in isocyanide complexes **6** and **7** at 2.6729(4) Å and 2.6840(4) Å, respectively, are slightly shorter than their CO analogues **4** and **5**, respectively.

Photophysical Properties. Figure 3 displays electronic spectra for $Ir^{I}Au^{I}$ complexes **1** and **3**; the spectrum of **2** is nearly identical to **1** and is shown in Supporting Information, Figure S1. The absorption profiles are dominated by the intense $d\sigma^* \rightarrow p\sigma$ transition, as has been assigned for other complexes of this type.[11,12] The transition is fairly metal localized as indicated by a minimal shift in the band maximum from 431 nm (ε = 17000 M^{-1} cm^{-1}) for **1** to 437 nm (ε = 18000 M^{-1} cm^{-1}) for **2**. Complex **3**, $[Ir^{I}Au^{I}(dppm)_2(CN^{t}Bu)_2](PF_6)_2$, shows an intense low-energy maximum at 490 nm (ε = 26000 M^{-1} cm^{-1}). Time-dependent DFT

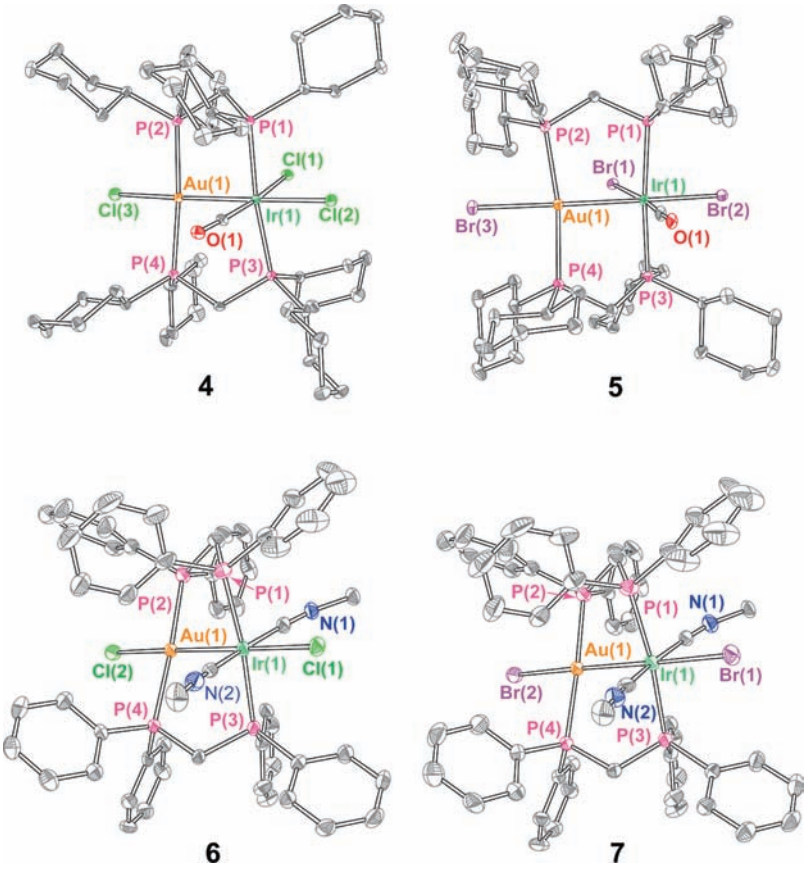

Figure 2. Thermal ellipsoid plots for **4**−**7**. Ellipsoids are shown at 50% probability level with counterions, solvent molecules, methyl groups, and hydrogen atoms omitted for clarity. Data was collected at 100 ± 2 K. The metal−metal distance is d(Ir−Au) = 2.6954(3) Å for **4**, d(Ir−Au) = 2.7096(4) Å for **5**, d(Ir−Au) = 2.6729(4) Å for **6**, and d(Ir−Au) = 2.6840(4) Å for **7**.

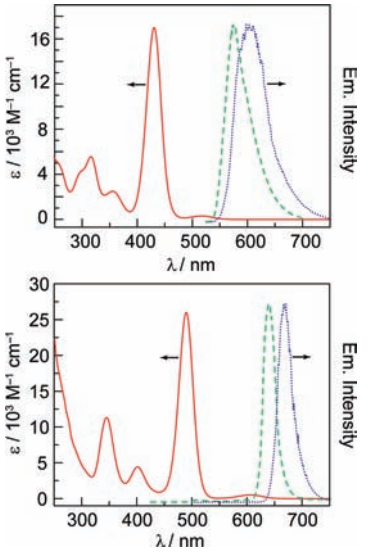

Figure 3. Overlaid absorption (red), glass emission (green), and solid-state emission (blue) spectra. The spectra of **1** are shown on top, and **3** on the bottom set of axes. The absorption spectrum was recorded at 293 K in CH_2Cl_2 solution. Emission spectra (λ_{exc} = 431 nm (**1**); 490 nm (**3**)) were recorded at 77 K; the frozen glass was of a 1:1 CH_2Cl_2/toluene solvent mixture.

calculations on the truncated phosphine model complexes $[Ir^IAu^I(dmpm)_2(CO)X]^+$ (X = Cl (**1′**); X = Br (**2′**)) and $[Ir^IAu^I(dmpm)_2(CNMe)_2]^{2+}$ (**3′**), where dmpm = bis(dimethylphosphino)methane, confirm the dσ^* → pσ nature of the intense low-energy transitions in **1**−**3**. Moreover, minimal halide contributions to the computed frontier orbitals of **1′** and **2′** are observed. Our results are consistent with recent computational findings on a series of Ir^IAu^I complexes.[15]

Table 2. Summary of 77 K Emission Data for Complexes **1**−**3**[a]

	solution[b]		solid state		
cmpd	λ_{em}/nm	τ/μs	λ_{em}/nm	τ_1/μs	τ_2/μs
1	575	9.8	605	0.81 (0.49)	6.7 (0.51)
2	582	9.8	620	0.55 (0.55)	4.0 (0.45)
3	640	6.8	670	0.67 (0.42)	3.6 (0.68)

[a] Parenthetical numbers represent the relative contributions of the two biexponential fitting parameters. [b] 4×10^{-5} M in 1:1 CH_2Cl_2/toluene.

The dσ^*pσ excited states of these complexes are emissive at 77 K, both in rigid solvent glass (1:1 CH_2Cl_2/toluene) and in the solid state (Figure 3 and Supporting Information, Figure S1). Emission data for all complexes are summarized in Table 2. The 77 K emission spectra in 1:1 CH_2Cl_2/toluene display maxima of 575 nm (**1**), 582 nm (**2**), and 640 nm (**3**), corresponding to Stokes shifts of 5800 cm^{-1} (**1**), 5700 cm^{-1} (**2**), and 4800 cm^{-1} (**3**), respectively. The emission is further red-shifted by about 1000 cm^{-1} in the solid state. Emission of samples in solvent glass decay monoexponentially (τ = 9.8 μs (**1**), 9.8 μs (**2**), and 6.8 μs (**3**)) whereas the emission decays of solid state samples are better approximated by a biexponential fit. The lifetimes and excited state characteristics of **1**−**3** are in line with previous studies on triplet state emission of Ir^IAu^I heterobimetallic complexes.[11−14]

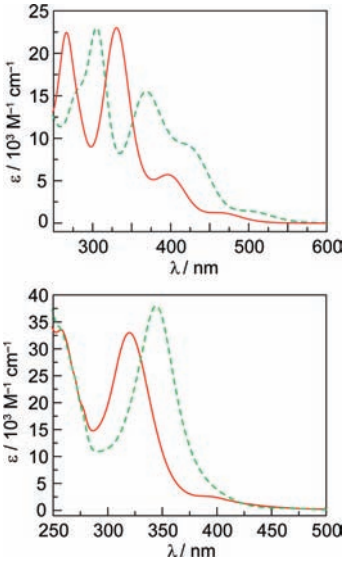

Figure 4. Overlaid electronic absorption spectra, measured in CH_2Cl_2 at 293 K. The spectra of **4** (red) and **5** (green) are shown on top, **6** (red) and **7** (green) on the bottom set of axes.

The spectral properties of the Ir^IAu^I core change markedly upon oxidation to $Ir^{II}Au^{II}$. Figure 4 displays overlaid absorption spectra for complexes **4**−**7**, measured at 293 K in CH_2Cl_2 solution. The most intense absorption features occur at significantly higher energies for the $Ir^{II}Au^{II}$ complexes. In all cases, these absorption maxima shift bathochromically upon substitution of bromide for chloride in otherwise isostructural complexes. The $Ir^{II}Au^{II}$ complexes are non-emissive at room temperature and 77 K, both in solution and in the solid state.

The electronic structure of the $Ir^{II}Au^{II}$ complexes was examined by DFT calculations. Model complexes were truncated by replacing all phenyl, cyclohexyl, and *tert*-butyl groups with methyl groups, and counterions were omitted ($[Ir^{II}Au^{II}(dmpm)_2(CO)X_3]^+$, X = Cl (**4′**); Br (**5′**) and $[Ir^{II}Au^{II}(dmpm)_2(CNMe)_2'X_2]^{2+}$, X = Cl (**6′**); Br (**7′**). Frequency calculations ensured that all optimized geometries represent minima on the potential energy surface. Metal−metal distances in the geometry-optimized models are consistently 0.06−0.10 Å longer than the observed distances from X-ray crystallography, but in general there is good agreement between calculated and observed structures. The orbital manifolds of **4′** and **5′** each contain two distorted σ-bonding orbitals responsible for the net metal−metal bond. The highest occupied molecular orbital (HOMO) is primarily derived from d orbitals with nearly equal contribution from the two metal atoms. The HOMO−7 also shows σ-orbital density between the metal atoms; this orbital is polarized toward the iridium and is of mixed d and p parentage, with considerable Au s contribution as well. In **6′** and **7′**, a single cylindrically symmetric σ-bonding orbital of mixed d and p parentage at the HOMO−2 level is responsible for the metal−metal bond. The HOMO in these complexes is a primarily iridium-centered dπ* orbital. The lowest unoccupied molecular orbital (LUMO) in **4′**−**7′** is the dσ* orbital, which is also σ-antibonding with respect to the axial halide ligands. Consistent with the sizable bathochromic shift that was observed in the absorption spectrum of the $Ir^{II}Au^{II}$ complexes upon substitution of chloride, the HOMO and other nearby filled orbitals for **5′** and **7′** are destabilized by ∼0.3 eV (Supporting Information, Figures S5−S6). These higher-lying occupied orbitals involve M—X σ* or π* interactions, which are responsible for the destabilization that occurs when chloride is replaced with bromide. In contrast, the LUMOs and other nearby virtual orbitals are very minimally perturbed.

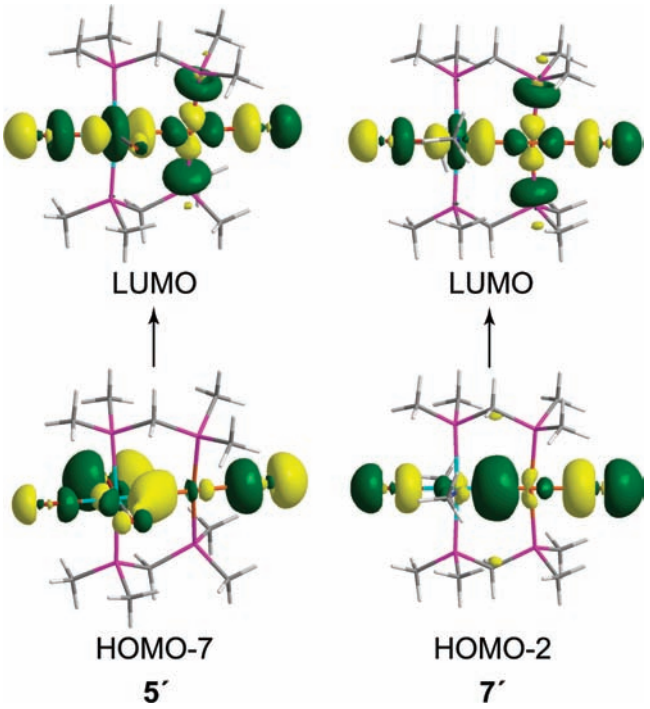

Figure 5. Plots for the predominant orbitals involved in the most intense electronic transitions of **5′** and **7′**, with contour levels of 0.04 au. Geometry optimizations were initiated from coordinates obtained from the crystal structures of **5** and **7**. Excitation energies (E = 3.69 eV for **5′** and E = 3.53 for **7′**) and oscillator strengths ($f_{336\ nm}$ = 0.38 for **5′** and $f_{351\ nm}$ = 0.53 for **7′**) were determined from time-dependent DFT calculations.

Time-dependent DFT calculations on the geometry optimized models provide insight into the nature of $Ir^{II}Au^{II}$ excited states. Calculations show that the most intense electronic transitions are primarily metal−metal $\sigma \rightarrow \sigma^*$ in character. Figure 5 shows the orbitals that are involved in this transition for bromide complexes **5′** and **7′**. The transitions involved in the analogous chloride complexes are essentially identical and are indicated pictorially in Supporting Information, Figure S2. The most intense electronic transition in **4′** and **5′** is between the HOMO−7, a distorted σ-bonding orbital of mixed d and p parentage, and the dσ* LUMO. This one-electron promotion comprises 74% (**4′**) and 81% (**5′**) of the excited state of the highest oscillator strength. The calculated transitions at 314 nm for **4′** and 336 nm for **5′** are reasonably close to the observed wavelengths of 331 and 369 nm for **4** and **5**. The transitions in **6′** and **7′** are also best described as (d,p)$\sigma \rightarrow$ dσ* and are reminiscent of the electronic transition calculated for an isostructural $Rh^{II}Au^{II}$ complex.[31] The most intense excitation in **6′** is calculated to occur at 328 nm, whereas that for **7′** at 351 nm. Again, these are reasonably close to the observed

(31) Esswein, A. J.; Dempsey, J. L.; Nocera, D. G. *Inorg. Chem.* **2007**, *46*, 2362–2364.

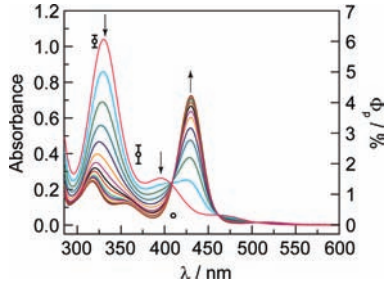

Figure 6. Spectral evolution during the photolysis of **4** with monochromic 320 nm light in CH_2Cl_2 with 2.2 M DMBD at 283 K. The open circles depict the values for the product appearance quantum yields, Φ_p, measured in 2.2 M DMBD as a function of excitation wavelength.

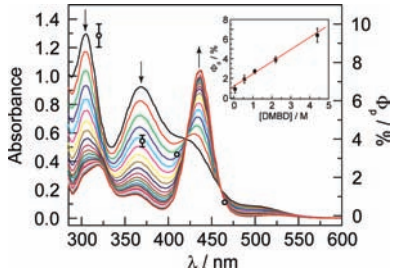

Figure 7. Spectral evolution during the photolysis of **5** with monochromic 370 nm light in CH_2Cl_2 with 2.2 M DMBD at 283 K. The open circles depict the values for the product appearance quantum yields, Φ_p, measured in 2.2 M DMBD as a function of excitation wavelength. The inset graph shows the dependence of the quantum yield on DMBD concentration with excitation provided at 370 nm.

transitions of 320 and 344 nm for **6** and **7**. The calculations also demonstrate that there is significant LMCT character in the low-energy transitions of **4′**−**7′**. In all cases, the Ir−Au σ-bonding orbital possesses substantial halide character, whereas the dσ* LUMO has greater metal character as a percentage of the total orbital composition. As a representative example, the HOMO−7 (d,p)σ orbital for **5′** has a 66.8% contribution from bromine atomic orbitals, but the dσ* LUMO is only 18.1% derived from bromine atomic orbitals.

Photochemistry. Irradiation of the $Ir^{II}Au^{II}$ complexes **4**−**7** in the presence of the halogen trap, 2,3-dimethyl-1,3-butadiene (DMBD), and with the exclusion of O_2, results in the prompt conversion of the photoreactants to the corresponding $Ir^{I}Au^{I}$ complexes.

Figure 6 depicts the evolution of the absorption spectrum when a CH_2Cl_2 solution of $[Ir^{II}Au^{II}(dcpm)_2COCl_3](PF_6)$, **4**, at 45 μM, is irradiated with monochromic 320 nm light in the presence of 2.2 M DMBD. Pristine isosbestic points are maintained at 408, 462, and 506 nm, indicating the absence of photochemical intermediates on a steady-state time scale. The final spectrum indicates quantitative production of the $Ir^{I}Au^{I}$ complex **1**. Clean formation of **1** is also observed when **4** is irradiated at other wavelengths within the photoreactant's absorption manifold. The dependence of the product-formation quantum yield, Φ_p, on the wavelength of excitation, with 2.2 M DMBD present, is also presented in Figure 6. The observed photochemical quantum yield decreases dramatically as the excitation energy is lowered. At 320 nm excitation, the observed quantum yield is 6.0(2)%, which decreases to 2.3(3)% at 370 nm and 0.30(3)% at 410 nm. At 465 nm excitation, negligible photoconversion is observed. The dependence of the quantum yield on DMBD concentration was investigated for λ_{exc} = 320 and 370 nm. In both cases, the quantum yields were found to be independent of trap concentration, over the range of 0.055 to 2.2 M for λ_{exc} = 320 nm[32] and 0.055 to 4.4 M for λ_{exc} = 370 nm.

The photochemistry of **5** largely parallels that observed for **4**. Figure 7 shows the changes in the absorption spectrum during the photolysis (λ_{exc} = 370 nm) of a CH_2Cl_2 solution containing $[Ir^{II}Au^{II}(dcpm)_2COBr_3](PF_6)$, **5**, at 60 μM and 2.2 M DMBD. Well-anchored isosbestic points are maintained but in this case at 421 and 461 nm, and the final photolysis spectrum reveals the quantitative formation of $Ir^{I}Au^{I}$ complex **2**. Clean photochemistry is reproduced at other excitation wavelengths that fall within the absorption manifold of **5** (Figure 4). The product appearance quantum yield of **5** decreases substantially as the excitation wavelength is increased, with values of 9.4(6)% at 320 nm, 3.9(3)% at 370 nm, 3.2(1)% at 410 nm, and 0.7(1)% at 465 nm, when the DMBD concentration is held at 2.2 M. In contrast to **4**, however, the photochemical quantum yield of **5** is sensitive to the DMBD concentration. As shown in the inset of Figure 7, the photochemical quantum yield increases linearly over the range of 0.055 to 4.4 M DMBD.

Photochemistry of $[Ir^{II}Au^{II}(dppm)_2(CN^tBu)_2X_2](PF_6)_2$, **6** and **7**, results in the formation of **3**, as judged by the changes to the UV−vis absorption spectra (see Supporting Information, Figures S3−S4). Photoproduct **3** is unstable to photolytic reaction conditions; the absorption bands of **3** bleach over extended irradiation times, and a colorless UV-absorbing species forms. Consistent with these observations, isosbestic points are not maintained over the course of photolysis of either **6** or **7**.

Discussion

The stable $Ir^{II}Au^{II}$ heterobimetallic complexes provide heretofore unknown examples of a direct iridium−gold bond in a bimetallic complex. The compounds are obtained with facility by halogen oxidation of parent $Ir^{I}Au^{I}$ complexes, which are furnished by following methods similar to that employed by Shaw and co-workers in their preparation of $[Ir^{I}Au^{I}(dppm)_2COCl]Cl$ by treating $[Ir^{I}(dppm)_2CO]Cl$ with $Au^{I}(PPh_3)Cl$ in boiling acetone.[9] We elected to use the Au^{I} starting material $Au^{I}(tht)X$, which is more labile and thus allows for milder reaction conditions. Considerable π back-donation from the Ir^{I} center is evident from the low energy of the C≡O stretching vibrations ($\tilde{\nu}_{CO}$ = 1944 and 1945 cm^{-1} for **1** and **2** vs, 2143 cm^{-1} for $^{12}C^{16}O$).[33] The CNMe analogue to **3** had been reported by ligand substitution on a pre-assembled $Ir^{I}Au^{I}$ complex.[12] The $Ir^{I}Au^{I}$ complex $[Ir^{I}Au^{I}(dppm)_2(CN^tBu)_2](PF_6)_2$, **3**, was prepared as previously described for isostructural $Rh^{I}Au^{I}$ complexes,[31] but initial attempts to prepare **3** by treatment of $[Ir^{I}Au^{I}(dppm)_2COCl](PF_6)$ with 2 equiv of CN^tBu resulted in a mixture of starting material, bis-CN^tBu and tris-CN^tBu complexes. The C≡N IR stretch

(32) UV absorption by DMBD precluded accurate quantum yield determination beyond 2.2 M when excited at 320 nm.

(33) Harris, D. C.; Bertolucci, M. D. *Symmetry and Spectroscopy: An Introduction to Vibrational and Electronic Spectroscopy*; Dover Publications: New York, 1978.

for **3** is observed at 2138 cm^{-1}, which is smaller than the value of 2306 cm^{-1} for free CN^tBu[34] and again indicates significant π back-donation.

Metal−metal bonding in the $Ir^{II}Au^{II}$ species is supported by all physical and spectroscopic characterization methods employed in this study. The C≡O and C≡N IR stretches shift by ∼50−60 cm^{-1} to higher energy, consistent with diminished π-back-donation resulting from oxidation of the bimetallic core. The crystal structures of these complexes show a contraction of the Ir−Au bond length that is indicative of direct metal−metal σ-bonding. The metal−metal bond length of **4**−**7** compare favorably with other d^7—d^9 third-row bimetallic complexes; they are slightly longer than structurally characterized $Pt^{III}Au^{II}$ [5] and $Pt^{III}Pt^{I}$ [6] complexes, and slightly shorter than isoelectronic $Ir^{II}Ir^0$ complexes.[8] The electronic structure of the $Ir^{II}Au^{II}$ core is also dominated by the metal−metal bond interaction. The most intense absorptions in **4**−**7** arise from metal−metal $\sigma \rightarrow \sigma^*$ transitions; the transition is Laporte allowed and consistent with the presence of an intense UV absorption. Moreover, the metal−metal bond shows characteristic mixing with the terminal halide ligands, especially from the halide axially coordinated along the metal−metal bond. The pronounced bathochromic shift in the absorption features upon substitution of chloride for bromide is indicative of substantial LMCT character in the excited state. The $Ir^{I}Au^{I}$ complexes show intense HOMO → LUMO absorptions that are primarily metal-centered. But in the reduced bimetallic core, the dσ^* orbital is filled and the metal based transition is of d$\sigma^* \rightarrow$ pσ character. As is typical of this type of excited state, [35−37] a pronounced emission is observed for both solution and solid-state samples of the $Ir^{I}Au^{I}$ complexes. With axial ligands removed from the metal−metal axis together with a reduced metal core, halide mixing into the metal based transitions of the $Ir^{I}Au^{I}$ complexes is greatly diminished. The absorption maximum of chloride-substituted **1** shifts by only ∼300 cm^{-1} in bromide-substituted **2**, consistent with a primarily metal-based transition devoid of significant halide character, an observation which is corroborated by time-dependent DFT calculations.

The presence of LMCT character in the lowest energy excited state of the $Ir^{II}Au^{II}$ complexes gives rise to a significant photochemistry. We have previously noted[5,6,38] that dσ^* excited states with heavily admixed LMCT character can promote the photoreductive elimination of halogen with the concomitant two-electron reduction of the metal core. The UV−vis spectroscopic features of the $Ir^{II}Au^{II}$ complexes establish that the same photochemistry is retained for $Ir^{II}Au^{II}$ cores. Complexes **4** and **5** cleanly reduce to **1** and **2**, respectively, when illuminated in the presence of a halogen trap. In both cases, the quantum yields for this photoreaction decrease substantially as the excitation wavelength is increased, as has been observed previously for d^7—d^9 bimetallic cores ligated by halide.[38] However, the dependence of quantum yield on the trap concentration for chloride-bound **4** and bromide-bound **5** is different. The photochemical quantum yield of **4** is invariant with respect to trap concentration over the range of 55 mM to 4.4 M DMBD, whereas the observed quantum yield for **5** increases linearly over the same range of concentrations. This divergent behavior suggests possible mechanistic differences in the photochemical transformations of the two complexes, which is currently under investigation with time-resolved spectroscopy.

In summary, we show that d^7—d^9 metal−metal bonded $Ir^{II}Au^{II}$ complexes are prepared by halogen oxidation of $d^8 \cdots d^{10}$ $Ir^{I}Au^{I}$ complexes. In contrast to thermally unstable tfepma-bridged $Rh^{II}Au^{II}$ complexes,[31] which are prepared by halogen transfer from tetrachloroaurate, the $Ir^{II}Au^{II}$ complexes described here are robust and their synthesis is general and straightforward. The $Ir^{II}Au^{II}$ complexes add to a growing library of d^7—d^9 species that photoeliminate X_2 by reductive elimination. Previous to the d^7—d^9 class of compounds, X_2 reductive elimination had not been observed from coordination or organometallic compounds. As demonstrated here for the $Ir^{II}Au^{II}$ complexes, the electronic structure of d^7—d^9 compounds, together with the low reorganization energy of the primary coordination sphere,[39,40] predisposes late transition metal heterobimetallic d^7—d^9 complexes to X_2 photoelimination, which is a key finding in overcoming the major impediment to achieving HX splitting photocatalysis.

Acknowledgment. This work was supported by NSF Grant CHE-0750239. Grants from the NSF also supported the MIT Department of Chemistry Instrumentation Facility (CHE-9808061, DBI-9729592). T.S.T. is grateful to the Fannie and John Hertz Foundation for a predoctoral fellowship. D.A.L. thankfully acknowledges the Jane Coffin Childs Memorial Fund for Medicinal Research for a postdoctoral fellowship.

Supporting Information Available: Electronic absorption and emission spectra of **2**, electronic transitions for **4′** and **6′** from time-dependent DFT, UV−vis traces for the photolysis of **6** and **7**, partial orbital energy level diagrams for **4′**−**7′**, Cartesian coordinates for the optimized geometries of **1′**−**7′**, the full citation for reference 23, and the crystallographic information file (CIF). This material is available free of charge via the Internet at http://pubs.acs.org.

(34) Spectral Database of Organic Compounds. http://riodb01.ibase.aist.go.jp/sdbs/cgi-bin/direct_frame_top.cgi (accessed July 2009), SDBS No. 18516.
(35) Che, C.-M.; Butler, L. G.; Gray, H. B.; Crooks, R. M.; Woodruff, W. H. *J. Am. Chem. Soc.* **1983**, *105*, 5492–5494.
(36) Che, C.-M.; Butler, L. G.; Gray, H. B. *J. Am. Chem. Soc.* **1981**, *103*, 7796–7797.
(37) Fordyce, W. A.; Brummer, J. G.; Crosby, G. A. *J. Am. Chem. Soc.* **1981**, *103*, 7061–7064.
(38) Heyduk, A. F.; Macintosh, A. M.; Nocera, D. G. *J. Am. Chem. Soc.* **1999**, *121*, 5023–5032.
(39) Veige, A. S.; Gray, T. G.; Nocera, D. G. *Inorg. Chem.* **2005**, *44*, 17–26.
(40) Gray, T. G.; Veige, A. S.; Nocera, D. G. *J. Am. Chem. Soc.* **2004**, *126*, 9760–9768.